Large-Eddy Simulation of Combustion Dynamics of Lean-Premixed Swirl-Stabilized Combustor

Ying Huang,[*] Hong-Gye Sung,[†] Shih-Yang Hsieh,[‡] and Vigor Yang[§]
Pennsylvania State University, University Park, Pennsylvania 16802

A comprehensive numerical study of the combustion dynamics in a lean-premixed swirl-stabilized combustor is described. The analysis treats the conservation equations in three dimensions and takes into account finite-rate chemical reactions and variable thermophysical properties. Turbulence closure is achieved using a large-eddy-simulation technique. The compressible-flow version of the Smagorinsky model is employed to describe subgrid-scale turbulent motions and their effect on large-scale structures. A level-set flamelet library approach is used to simulate premixed turbulent combustion. The governing equations and the associated boundary conditions are solved by means of a four-step Runge-Kutta scheme along with implementation of the message passing interface parallel computing architecture. The analysis allows for a detailed investigation into the interaction between turbulent flow motions and oscillatory combustion of a swirl-stabilized combustor. Several physical processes responsible for driving combustion instabilities in the chamber have been identified and quantified, including the mutual coupling between acoustic wave motions, vortex shedding, and flame oscillations. In particular, the mechanisms of energy transfer from chemical reactions in the flame zone to acoustic motions in the bulk of chamber are carefully studied.

Nomenclature

C_R, C_I	=	empirical constants
C	=	speed of sound, m/s
D	=	Van-Driest damping function
E	=	specific total energy
f	=	frequency, Hz
G	=	level-set variable
$h^0_{f,i}$	=	heat of formation of species i at reference condition
k	=	turbulent kinetic energy
l_F	=	laminar flame thickness, m
l_δ	=	inner-layer flame thickness, m
$\boldsymbol{n}$	=	unit vector normal to flame front
p	=	pressure
P_r	=	Prandtl number
q	=	rate of heat release per unit volume
R	=	gas constant
$\Re e$	=	real part of a complex variable
R_c	=	radius of combustor chamber
R_h	=	radius of center body (inner radius of inlet annulus)
R_n	=	outer radius of inlet annulus
S	=	flame speed, or swirl number
S_{ij}	=	strain-rate tensor
S_r	=	strouhal number
u_i	=	velocity, m/s
u_τ	=	friction velocity, m/s
Y_i	=	mass fraction of species i
y^+	=	normalized distance from wall
γ	=	ratio of specific heats
Δ	=	filter width
δ_{ii}	=	Kronecker delta
η	=	Kolmogorov length scale, m
θ	=	phase angle
μ	=	dynamic viscosity, kg/ms
ρ	=	density, kg/m^3
τ_{ii}	=	viscous shear stress, N/m^2
ϕ	=	equivalence ratio
φ	=	swirl vane angle
ω	=	vorticity, 1/s

Subscripts

A	=	acoustic property
L	=	laminar property
rms	=	root mean square
T	=	turbulent property

Superscripts

sgs	=	subgrid scale
−	=	ensemble averaging
~	=	favre averaging
′	=	fluctuation

I. Introduction

G AS-TURBINE engines have traditionally used diffusion-flame combustors because of their reliable performance and reasonable stability characteristics. Unfortunately, this type of combustor produces unacceptably high levels of thermal NO_x. The increasingly strict regulation of pollutant emissions has recently urged engine manufacturers to turn to lean premixed (LPM) combustion as an effective means to fulfill the regulatory requirements.[1,2] In LPM combustion, the fuel and air are premixed upstream of the combustor to avoid toe formation of stoichiometric regions. The combustion zone is operated with excess air to reduce the flame temperature, and consequently thermal NO_x is virtually eliminated. However, unsteady flow oscillations, usually referred to as combustion instability or dynamics, have emerged as a common problem and hindered the development of LPM combustors. These oscillations in the flowfield may reach sufficient amplitudes to interfere with engine operation. In extreme cases, the ensuing structural vibration and excessive heat transfer to the chamber lead to failure of the system.

Combustion instabilities may be regarded as the unsteady motions in a dynamical system capable of sustaining large oscillations over a broad range of frequencies. Because fluctuations arise from causes internal to the system, they are true instabilities and an external observer perceives the result as the dynamical behavior of a self-excited system. Instabilities in different systems are distinguished primarily by the geometry and the manner in which the reactants are introduced. The prevalence of instabilities is primarily attributed to two fundamental phenomena:[3,4]

1) Combustion chambers are almost entirely closed and the internal processes tending to attenuate unsteady motions are weak.

2) The energy required to drive unsteady motions represents an exceedingly small fraction of the heat released by combustion.

These underlying issues are present in any combustion chamber, but are especially consequential for gas-turbine engines, in which energy intensity is extremely high, typically of the order of 100 $MW/m^3/bar$. In typical instances, less than 0.1% of the energy released in chemical reactions is sufficient to generate pressure fluctuations having peak amplitudes equal to the mean chamber pressure.

Clearly, a comprehensive understanding of combustion instability is strongly needed. Although the energy needed to drive unsteady motions is exceedingly small compared with the heat release from chemical reactions, combustion instabilities cannot be sustained unless a certain dynamic relation between heat-release fluctuations and acoustic flow oscillations is satisfied in the chamber. This relationship was first identified by Lord Rayleigh and is now well known as the Rayleigh criterion. Several mechanisms responsible for driving combustion instabilities such as vortex shedding[5] and equivalence-ratio fluctuations,[6] which modify either the heat release fluctuations or the local flow oscillations or both, have been proposed and studied. Very limited effort, however, has been expended to investigate the detailed flame dynamics, especially at scales sufficient to resolve the energy transfer process in an oscillatory environment. Most LPM systems stabilize the flame with recirculation developed by swirling flows for the purpose of clean and efficient combustion. There are, however, many unresolved issues with respect to swirling flows, such as swirl generation, vortex breakdown, axisymmetry breaking, and azimuthal instability.[7,8] Effects of swirling flow on combustion instabilities remain largely unclear, at least in the quantitative sense. The lack of fundamental information about the flame/flow interaction has seriously jeopardized the establishment of a knowledge-based design methodology to cure the instability problem. The present work attempts to address this issue numerically by means of a large-eddy-simulation (LES) technique, with special attention given to the turbulent flame dynamics in a lean-premixed swirl-stabilized combustor. The specific objectives are (1) to develop and implement a level-set flamelet library approach for premixed turbulent flames in the context of LES and (2) to investigate system-atically the key mechanisms responsible for driving and sustaining combustion oscillations in a single LPM swirl injector.

LES techniques may be viewed as the next step in addressing fluid mechanics problems where classical Reynolds-Averaged Navier-Stokes (RANS) modeling fails to deliver accurate results. LES techniques compute explicitly the contributions of large energy-carrying structures to mass, momentum, and energy transfer in the flowfield, with the effects of unresolved small-scale turbulence modeled either analytically or empirically. They are well suited for studying gas-turbine combustion dynamics, since the flowfield of concern is highly unsteady and dominated by turbulence motions that can be adequately resolved computationally.

Several attempts have been made to study combustion dynamics using LES. Menon and Jou[9] conducted a pioneering two-dimensional LES of combustion dynamics in an axisymmetric ramjet combustor. Results were able to capture globally the unstable flame evolution observed in experiments. Kailasanath et al.[10] also investigated the combustion dynamics in an axisymmetric ramjet combustor. Both reacting and no-reacting flows were simulated. The reacting flow calculations showed that heat release from chemical reactions amplified the low-frequency oscillations observed

in the non-reacting flow. Thibaut and Candel[11] studied the flashback phenomena in a backward-facing step configuration using a two-dimensional analysis. The mechanism of flashback associated with combustion dynamics was investigated. Schonfeld and Poinsot[12] studied the influences of initial and boundary conditions on premixed combustion instabilities in a gas-turbine burner. Kim et al.[13] investigated a swirl-stabilized gas-turbine combustor flow. A complex vortex shedding pattern with significant azimuthal structures was clearly identified. Angelberger et al.[14] conducted a two-dimensional simulation of a premixed dump combustor with acoustic forcing. Fureby[15] investigated the combustion instabilities in a dump combustor and a model afterburner. Vortex shedding was found to be the main contribution to driving combustion instabilities. Wang et al[16] recently examined the vortical flow dynamics in swirl injectors with radial entry. Various flow instability mechanisms, including the Kelvin-Helmholtz, helical, and centrifugal instabilities, as well as their mutual interactions, were investigated in detail.

II. LES Combustion Models for Premixed Turbulent Flames

In treatment of turbulent reacting flows within the context of LES, detailed flame structures are often not resolved, and combustion models are needed on the subgrid scales (sgs).[17] Modeling of the sgs reaction-rate term using the Arrhenius law based on filtered quantities (i.e., no sgs combustion model) often under-predicts the global turbulent burning rate (since the unresolved flame is wrinkled at scales below the LES resolution, which typically increases the global reaction rate[18]), and thus may lead to unexpected flame blow-off.[19] Table 1 summarizes a variety of approaches that have recently been employed to perform LES of premixed turbulent combustion. These models can be broadly classified into two categories: flamelet and non-flamelet models. Flamelet models, such as flame surface density-approach, flame-wrinkling model and level-set model, generally assume chemical reactions to be confined in a thin, sheet-like laminar flame structure whose inner layer is unaffected by turbulence, a situation that occurs in many combustion systems.[20,21] In the following, the combustion models listed in Table 1 will be briefly reviewed.

Eddy-break-up type models[17] usually assume that fuel reaction rate is controlled by the characteristic turbulent time scale, although chemical time scale can be included. The models often tend to over-estimate the reaction rate within the context of RANS.[22-24] For LES, the model constants seem to be strongly dependent on flow conditions and numerical mesh size.[17,22] In thickened-flame models,[11,14,18,25] the flame is artificially broadened by increasing the thermal diffusivity, while keeping the flame propagating properties (i.e. flame speed) unchanged by reducing the reaction rate. The resultant thickened flame can thus be resolved on the LES grid using the Arrhenius law. Thickened-flame models are widely used because of their capability of treating complex chemistry and transient phenomena such as ignition, extinction, and flame-wall interaction. As indicated by Colin et al.,[25] however, the Damköhler number (defined as the ratio of turbulent time scale to chemical time scale) is changed in this approach, and the ensuing modification of the flame response to turbulent motions may introduce some unknown effects on the simulation of combustion dynamics.

In the linear eddy model,[26,27] the large-scale, resolvable scalar processes are simulated explicitly on the LES grid, while sgs turbulent processes and chemical reactions occurring within each numerical cell are treated using a one-dimensional model. This approach is complex and can be time-consuming, since the one-dimensional model is used in each cell and the advection of scalars between LES cells requires additional treatment. In the flame surface-density approach,[19,21,28] flame-wrinkling model,[29,30] and turbulent flame-speed closure model,[31] a filtered progress variable is usually solved. The unclosed reaction source term is modeled by introducing an sgs flame-surface density, an sgs flame-wrinkling factor (defined as the ratio of the sgs flame surface area to its projection in the propagation direction) or an sgs turbulent flame speed, respectively. The first two parameters can be obtained from either an algebraic expression[18,19,32] or a balance equation,[28] and the

Table 1 Survey of LES Combustion Models for Premixed Turbulent Flame

Model description	Application	References	Remarks
Eddy-breakup type	Triangular-shaped bluff body	Fureby and Lofstrom[22] Fureby and Moller[23] Moller et al.[24]	filtered reaction rate determined by sgs mixing and chemical kinetics
Thickened flame	Backward facing step; premixed dump combustor; premixed flame in decaying isotropic turbulent flow	Thibaut and Candel[11] Angelberger, et al.[14] Charlette, etc.[18,32] Colin et al.[25]	Arrhenius law used for artificially thickened flame
Linear eddy	Turbulent stagnation point premixed flame	Chakravarthy and Menson[26,27]	Small-scale turbulence and chemical process treated using a one-dimensional model
Flame surface-density	Freely propagating turbulent premixed flame	Hawkes and Cant[21,28]	Filtered reaction rate modeled by introducing flame surface density
Flame-wrinkling	Rearward-facing step; triangular-shaped bluff body	Weller, et al.[29] Fureby[30]	Filtered reaction rate estimated using flame wrinkling factor
Turbulent flame-speed closure	Backward-face step combustor	Flohr and Pitsch[31]	Turbulent flame speed used to model filtered reaction term
G-equation based on progress variable	Swirl-stabilized gas-turbine combustor	Kim et al.[13]	Flame front evolution described using G-equation based on progress variable
Level-set	Turbulent Bunsen burner	Duchamp de Lageneste and Pitsch[35]	Flame front evolution governed by a level-set equation

last parameter from existing theoretical and experimental data for turbulent flame speed. In general, modeling of these three terms is closely related to flame wrinkling effects caused by unsolved turbulent motions.

The G-equation approach attempts to describe the premixed turbulent combustion from a geometrical point of view. The flame front is represented by an arbitrary iso-surface G_0 in a scalar field G whose evolution is formulated using the so-called G-equation. Since the G-field outside the flame front is not uniquely defined, several approaches can be used. Menon and his colleagues[9,13] regarded G as a progress variable (i.e., G = 0 and 1 for the fresh unburnt and burnt gases, respectively). The model is simple and easy to implement, but, as is pointed out in Refs. 9 and 13, the numerical difficulties and grid resolution may incorrectly broaden the flame. Peters,[20] on the other hand, proposed a level-set approach which defines G as a distance function outside the flame front, where the flame front position is given by G = 0. This approach, along with a laminar flamelet library and a presumed PDF method, offers a more realistic treatment of premixed turbulent flame dynamics. Another advantage of the level-set approach is that chemistry is decoupled computationally from turbulence and the difficulty of modeling turbulent chemical reaction rates can be thus avoided.

The level-set approach has been extensively explored by Peters in his monograph[20] and tested by Herrmann[33] and Bai and Nilsson[34] within the context of RANS. Its application to LES seems promising and has recently received substantial attention,[35,36] and will be implemented in the present study.

III. Theoretical Formulation

The physical model of concern is shown in Fig. 1. It includes an axisymmetric chamber connected upstream with a swirl injector and downstream with a choked nozzle, simulating the experimental facility described in Refs. 37 and 38. Lean premixed air and methane gases are delivered to the chamber through eight straight, flat vanes with an angle of 45 degrees relative to the incoming flow. Following common practice, the swirl number S is defined as the ratio of the axial flux of the tangential momentum to the product of the axial momentum flux and a characteristic radius.

$$S = \int_{R_h}^{R_n} \overline{u}\,\overline{w}r^2 dr \bigg/ \int_{R_h}^{R_n} R_n \overline{u}^2 r dr \qquad (1)$$

where R_h and R_n are the inner and outer radii of the inlet annulus, respectively. If we assume that the axial and azimuthal velocities are uniform and the vanes are very thin, the swirl number can be written as:
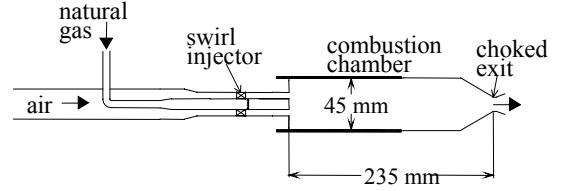
Fig. 1 Schematic of a model swirl-stabilized gas-turbine combustor (after Broda et al.[37]).

$$S = \frac{2}{3}\left[\frac{1-(R_h/R_n)^3}{1-(R_h/R_n)^2}\right]\tan\varphi \qquad (2)$$

where φ is the swirler vane angle. The estimated swirl number is 0.76 for a 45-deg swirler with a constant chord and vane angle, which is in the category of high-swirl number (approximately $S \geq 0.6$).[39] Natural gas is injected radially from the center body through ten holes immediately downstream of the swirler vanes. The fuel/air mixture is assumed to be well mixed before entering the combustor (perfect premixing assumption is used here to isolate the effects of equivalence-ratio fluctuations on combustion dynamics). The chamber measures a diameter of 45 *mm* and a length of 235 *mm* through the nozzle throat. The choked nozzle at the exit prevents any downstream disturbances from traveling upstream and maintains the desired chamber pressure. A choked venturi is also installed at the inlet entrance to acoustically isolate the test section from the air supply line.

A. Governing Equations

The formulation is based on the Favre-filtered conservation equations of mass, momentum and energy in three dimensions. These equations are obtained by filtering the small-scale dynamics from the resolved scales over a well-defined set of spatial and temporal intervals. They can be conveniently expressed in the following Cartesian tensor form

$$\frac{\partial \overline{\rho}}{\partial t} + \frac{\partial \overline{\rho}\tilde{u}_j}{\partial x_j} = 0 \qquad (3)$$

$$\frac{\partial \overline{\rho}\tilde{u}_i}{\partial t} + \frac{\partial(\overline{\rho}\tilde{u}_i\tilde{u}_j + \overline{p}\delta_{ij})}{\partial x_j} = \frac{\partial(\overline{\tau}_{ij} - \tau_{ij}^{sgs})}{\partial x_j} \qquad (4)$$

$$\frac{\partial \overline{\rho}\tilde{E}}{\partial t} + \frac{\partial((\overline{\rho}\tilde{E} + \overline{p})\tilde{u}_i)}{\partial x_i} = \frac{\partial}{\partial x_i}\left(\tilde{u}_j\overline{\tau}_{ij} + \overline{q}_i - H_i^{sgs} + \sigma_{ij}^{sgs}\right) \qquad (5)$$

where overbars and tildes denote resolved-scale and Favre-averaged resolved-scale variables, respectively. In the preceding equations, τ_{ij} and q_i are the viscous stress tensor and heat flux, respectively. A detailed derivation of the filtered equations is presented in Oefelein and Yang.[40] The unresolved *sgs* terms in Eqs. (3–5), including the *sgs* stresses term τ_{ij}^{sgs}, the *sgs* energy fluxes term H_i^{sgs} and the *sgs* viscous work term $\sigma_{i,j}^{sgs}$, are given as

$$\tau_{ij}^{sgs} = (\overline{\rho u_i u_j} - \overline{\rho}\widetilde{u}_i\widetilde{u}_j) \tag{6}$$

$$H_i^{sgs} = (\overline{\rho E u_i} - \overline{\rho}\widetilde{E}\widetilde{u}_i) + (\overline{p u_i} - \overline{p}\widetilde{u}_i) \tag{7}$$

$$\sigma_{ij}^{sgs} = (\overline{u_j \tau_{ij}} - \widetilde{u}_j \widetilde{\tau}_{ij}) \tag{8}$$

The *sgs* shear stress is modeled using the compressible version of the Smagorinsky model suggested by Erlebacher et al.[41]

$$\tau_{ij}^{sgs} = -2\nu_t \overline{\rho}(\widetilde{S}_{ij} - \frac{\widetilde{S}_{kk}\delta_{ij}}{3}) + \frac{2}{3}\overline{\rho}k^{sgs}\delta_{ij} \tag{9}$$

where

$$\nu_t = C_R(D\Delta)^2(2\widetilde{S}_{ij}\widetilde{S}_{ij})^{1/2} \tag{10}$$

$$k^{sgs} = C_I(D\Delta)^2(2\widetilde{S}_{ij}\widetilde{S}_{ij}) \tag{11}$$

The two dimensionless constants, $C_R(\approx 0.01)$ and $C_I(\approx 0.007)$, are determined empirically, $k^{sgs} = \tau_{kk}^{sgs}/2\overline{\rho} = (\overline{\rho u_k u_k}/\overline{\rho} - \widetilde{u}_k\widetilde{u}_k)/2$ and $\widetilde{S}_{ij} = (\partial\widetilde{u}_i/\partial x_j + \partial\widetilde{u}_j/\partial x_i)/2$. The Van-Driest damping function D is used to account for the inhomogeneities near the wall,

$$D = 1 - \exp\left(1 - (y^+)^3/26^3\right) \tag{12}$$

where $y^+ = yu_\tau/\nu$. The *sgs* energy flux H_j^{sgs} is modeled as

$$H_j^{sgs} = -\overline{\rho}\frac{\nu_t}{Pr_t}\left(\frac{\partial\widetilde{h}}{\partial x_j} + \widetilde{u}_i\frac{\partial\widetilde{u}_i}{\partial x_j} + \frac{1}{2}\frac{\partial k^{sgs}}{\partial x_j}\right) \tag{13}$$

A standard value of 0.7 is used for the turbulent Prandtl number. The unclosed *sgs* viscous work term $\sigma_{i,j}^{sgs}$ is assumed to be small and is neglected in the present study. The filtered total energy $\widetilde{E}$ can be modeled as:

$$\widetilde{E} = \widetilde{\psi} + \int_{T_{ref}}^{\widetilde{T}} C_p(T')dT' - \overline{p}/\overline{\rho} + \frac{\widetilde{u}_k^2}{2} + k^{sgs} \tag{14}$$

where $\psi = \sum_{k=1}^{N} Y_k \Delta h_{f,k}^0$

B. Level-Set Flamlet-Library Combustion Model

Premixed turbulent combustion involves a wide range of length and time scales associated with chemical reactions and flow motions. Peters[20] examined the problem of turbulence/chemistry interactions in terms of two non-dimensional parameters, turbulent Reynolds number *Re* and turbulent Karlovitz number *Ka*, as defined below

$$Re \approx v'l/S_L/l_F \tag{15}$$

$$Ka = t_F/t_\eta \approx l_F^2/\eta^2 \tag{16}$$

where v' is turbulent velocity fluctuation, l turbulent integral length scale, S_L and l_F the flame speed and thickness, respectively, t_F and t_η the flame and the Kolmogorov time scales, respectively, and η the Kolmogorov length scale. Another Karlovitz number Ka_δ, defined as the square of ratio of the flame inner layer thickness l_δ to the Kolmogorov length scale η, is also introduced. Based on the relative magnitudes of these parameters, premixed turbulent combustion can be classified into four different regimes, as shown in Fig. 2. Corrugated flamelets occur when $Re > 1$, $v'/S_L > 1$ and $Ka < 1$. In this regime, turbulent velocity fluctuation v' is large
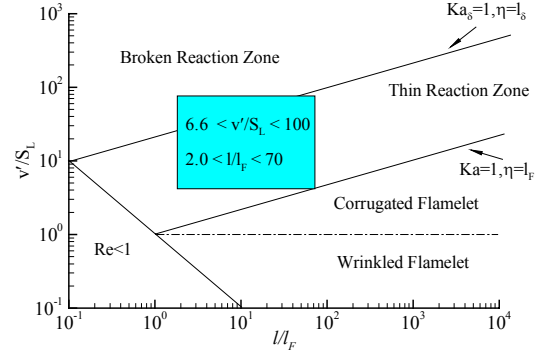
Fig.2 Regime diagram of premixed turbulent combustion (after Peters[20]).

enough to allow eddies to corrugate the flame front. The smallest eddies of size η, however, are still larger than the laminar flame thickness l_F, and thus cannot modify the flame structure. The interaction between eddies of all sizes and the laminar flame structure is purely kinematic. The chemical and transport processes within the flame remain essentially unchanged. A thin reaction zone exists when $Re > 1$, $v'/S_L > 1$, $Ka > 1$ and $Ka_\delta < 1$. In this regime, the smallest eddies of size η are smaller than the laminar flame thickness l_F, and can penetrate into the bulk of the flame structure. They cannot, however, enter into the inner layer because the smallest eddies are larger than the thickness of the inner layer. Although the local transport of chemical species and energy are enhanced in the preheat zone, the chemical reactions that sustain the flame are essentially uninfluenced by turbulence since they do not penetrate into the inner layer. The wrinkled flamelet regime ($Re > 1$, $v'/S_L < 1$ and $Ka < 1$) and the broken reaction zone ($Re > 1$, $v'/S_L > 1$, and $Ka_\delta > 1$) are two extreme situations with very weak turbulence intensity or with very small turbulence eddies, which can alter the chemical reactions in the inner layer. In this work, the last two regimes will not be discussed and the flamelet assumption will be employed.

In both the thin reaction and corrugated-flamelet regimes, the inner layer of the laminar flame structure is not affected by turbulence. Therefore, based on the level-set flamelet approach, the premixed turbulent flame can be treated as a synthesis of thin reaction-diffusion layers, commonly referred as flamelets,[33] embedded in an otherwise inert turbulent flow field. When a Reynolds-average approach is used, the turbulent flame is viewed as the ensemble average of different laminar flamelets, which fluctuate randomly around the mean flame position in the normal direction under the effect of turbulence. For LES, the filter process is considered as a local volume average.[42] The filtered mean flame also can be regarded as the average of different laminar flamelets, which randomly fluctuate around the mean flame position in the normal direction under the effects of unresolved small-scale turbulence. The mean location of flamelets is obtained by solving a level-set transport equation. After the structure of the laminar flamelet is determined by employing a finite-rate chemistry model, a presumed PDF method can be used to determine the mean thermophysical properties, such as species concentrations.

1. Level-Set Equation for Premixed Turbulent Flame

A scalar-field G equation describing the evolution of a thin flame front can be written as.

$$\partial\rho G/\partial t + \nabla \cdot \rho\mathbf{u}G = \rho S_L |\nabla G| \tag{17}$$

where the laminar flame speed S_L for an idealized planar configuration depends on pressure, temperature, and mixture equivalence ratio.[43] In reality, flame curvature and flow unsteadiness, which can be characterized by a stretch rate κ [defined as the fractional rate of change of a flame surface area $\kappa = (d\delta A/dt)/\delta A$], have a significant impact on the flame speed S_L.[44,45] Depending on the Lewis number, the stretch rate can increase or decrease the flame

speed. A linear model[44] for small stretch has been proposed to account for this effect.

$$S_L = S_L^0 - S_L^0 M\kappa \tag{18}$$

where S_L^0 is the laminar burning velocity of a plane, undisturbed premixed laminar flame, and M the Markstein length, which is a function of mixture properties. When Eq. (17) is filtered, the following Favre-averaged G-equation for LES is obtained:

$$\partial \overline{\rho}\widetilde{G} / \partial t + \nabla \cdot \overline{\rho \mathbf{u}}\widetilde{G} = -\nabla \cdot (\overline{\rho \mathbf{u}G} - \overline{\rho}\widetilde{\mathbf{u}}\widetilde{G}) + \overline{\rho S_L \mid \nabla \widetilde{G} \mid} \tag{19}$$

The first term on the right-hand side of Eq. (19) is associated with turbulent transport. Since the original G equation is parabolic, this term cannot be approximated using a classical gradient-transport approach because of the reduction to an elliptic equation for $\widetilde{G}$. According to Peters,[20] it is modeled as:

$$\nabla \cdot (\overline{\rho \mathbf{u}G} - \overline{\rho}\widetilde{\mathbf{u}}\widetilde{G}) = \overline{\rho}D_t \widetilde{k} \mid \nabla \widetilde{G} \mid \tag{20}$$

where $D_t = v_t / \mathrm{Pr}_t$ and $\widetilde{k}$ is the filtered flame front curvature, $\widetilde{k} = \nabla \cdot \widetilde{\mathbf{n}} = \nabla \cdot (-\nabla \widetilde{G} / \mid \nabla \widetilde{G} \mid)$. The second term on the right-hand side of Eq. (19) represents turbulent flame propagation and can be related to the *sgs* turbulent flame speed S_T as follows

$$\overline{\rho S_L \mid \nabla G \mid} = \overline{\rho}S_T \mid \nabla \widetilde{G} \mid \tag{21}$$

Substitution of Eqs. (20) and (21) into Eq. (19) leads to a modeled filtered G equation.

$$\partial \overline{\rho}\widetilde{G} / \partial t + \nabla \cdot \overline{\rho}\widetilde{\mathbf{u}}\widetilde{G} = \overline{\rho}S_T \mid \nabla \widetilde{G} \mid -\overline{\rho}D_t \widetilde{k} \mid \nabla \widetilde{G} \mid \tag{22}$$

The *sgs* turbulent flame speed S_T needs to be treated. This closure generally takes the form[46]

$$S_T = S_L (1 + C(v'_\Delta / S_L)^n) \tag{23}$$

where v'_Δ is the *sgs* turbulent velocity fluctuation and may be modeled as $v'_\Delta = 2.0\Delta^3 (\nabla \times (\nabla^2 \widetilde{\mathbf{u}}))$.[25] The two constants C and n need be specified ($C \approx 2.0$, $n \approx 0.7$) or dynamically determined.

2. Presumed PDF Methods

With the assumption that mean turbulent flame is an ensemble average or local volume average of different laminar flamelets which fluctuate randomly around the mean flame position in the normal direction under the effect of turbulence, the mean chemical composition of a premixed turbulent flame can be obtained using a presumed PDF method along with a resolved flamelet structure. To this end, the probability of finding the instantaneous flame front at a given position and instant needs be presumed. A reasonable choice appears to be a Gaussian distribution.[20,47,48]

As mentioned before, the filtered G equation is valid only for the flame front, but the entire flow-field. A re-initialization condition $\mid \nabla \widetilde{G} \mid = 1$ can be applied away from the flame and renders $\widetilde{G}$ a distance function normal to the flame surface. Once $\widetilde{G}$ is defined, the turbulent flame thickness $l_{F,t}$, which measures the flame front fluctuations in the normal direction, can be defined as

$$l_{F,t} = (\overline{G''^2})^{1/2}_{\widetilde{G}=G_0} \tag{24}$$

where $(\overline{G''^2})^{1/2}_{\widetilde{G}=G_0}$ is a conditional variance evaluated at the flame front $\widetilde{G} = G_0$. Note that the flame thickness can only be defined at the flame surface. Then a Gaussian-shaped PDF can be obtained:

$$P(G;\mathbf{x},t) = \frac{1}{[2\pi(\overline{G''^2})_0]^{1/2}} \exp\{-\frac{[G - \widetilde{G}(\mathbf{x},t)]^2}{2(\overline{G''^2})_0}\} \tag{25}$$

Here the effects of strain on the flame structure and orientation between the instantaneous and mean flame surfaces are not included.

The averaged mass fraction of species i can be calculated by

$$\widetilde{Y}_i(\mathbf{x},t) = \int_{-\infty}^{\infty} Y_i(G,t)P(G,\mathbf{x},t)dG \tag{26}$$

However, in order to obtain a presumed PDF, information about the flame thickness or the G variance is needed. The filtered flame thickness $l_{F,t}$ is determined by the fluctuation of laminar flamelets under the effect of unresolved small-scale turbulence. A transport equation for the filtered G variance can be derived. But such a model is yet to be developed within the context of LES. A simple approach based on dimensional analysis is thus implemented here. The *sgs* flame thickness $l_{F,t}$ is a function of the laminar flame thickness l_F, filter width Δ, *sgs* turbulent velocity fluctuation v'_Δ and other parameters.

$$l_{F,t} = f(l_F, \Delta, v'_\Delta, ...) \tag{27}$$

In the limit of an infinitely thin flame, the *sgs* flame thickness $l_{F,t}$ will become independent of laminar flame thickness l_F.

$$l_{F,t} = f(\Delta, v'_\Delta, ...) \tag{28}$$

Peters[20] proposed a simple model in the context of RANS, $l_{F,t} \approx Cl$, where l is the integral length scale and C is a constant. A similar approach is taken for LES accordingly.

$$l_{F,t} = C_0\Delta + l_F \tag{29}$$

where $C_0 (\approx 1)$ is an empirical constant. The model suffers from a major limitation that the effects of small-scale motions on flame thickness are totally represented by the filter width, a situation rather remote from reality. A transport equation for the G variance is required in order to correctly address this problem.

3. Generation of Laminar Flamelet Library

By assuming that a turbulent premixed flame is a collection of flamelets embedded in an otherwise inert turbulent flow field, the inner structure of a premixed flame can be calculated separately from the turbulent flow calculation, taking into account finite-rate chemistry and elementary reaction mechanisms. There are several ways to generate a laminar flamelet library. The simplest approach is to assume infinitely fast chemistry and a quasi-laminar flame without an inner structure. All of the flow quantities change abruptly from the unburned to the burned state. Unfortunately, this neglects the effects of finite-rate chemistry and transport phenomena inherent in a flame.

Another way to determine the inner structure of a flame is to solve flamelet equations,[20] valid for both the corrugated-flamelet and the thin-reaction regions in the regime diagram for premixed turbulent combustion. This approach is not used because of its complexity. In the present study, the flamelet library is established by solving a system of transport equations for the temperature and species-concentration fields for a freely propagation plane flame. The entire flame is assumed to be laminar without the influence of turbulence. This method, originally proposed by Nilsson and Bai,[34] is adopted here because of its ease of implementation.

4. Re-initialization Process

The $\widetilde{G}$ variable is defined as a distance function outside the flame front, but this property is not conserved by the level-set equation. It needs to be enforced by a re-initialization process. From the numerical point of view, because the discretization of the level-set equation contains the spatial gradients of $\widetilde{G}$, a dependency on values of $\widetilde{G} \neq \widetilde{G}_0$ near the flame surface is introduced. It is important to keep the values of the gradient of G near unity in order not to undermine the numerical accuracy.[33] Several methods have been proposed to enforce the condition $\mid \nabla \widetilde{G} \mid = 1$ and render the level-set function a signed distance (with negative distance on one side and positive distance on the other side). The method developed by Sussman et al.[49] and Russo et al.[50] with a narrow banding

strategy[51] is used here, by solving the following equations iteratively to a steady-state.

$$\partial \widetilde{G} / \partial \tau = \mathrm{sgn}(\widetilde{G}_0)(1 - |\nabla \widetilde{G}|), \qquad \widetilde{G}(\mathbf{x},0) = \widetilde{G}_0(\mathbf{x}) \qquad (30)$$

where $\mathrm{sgn}(\widetilde{G}_0)$ is a smoothed sign function. The steady solution satisfies the condition of $|\nabla \widetilde{G}| = 1$ and has the same zero-level as $\widetilde{G}_0$. Thus the desired signed distance function is obtained.

The coupling of the flow equations and the flamelet library is treated following the approach by Herrmann.[33] The thermophysical variables extracted from the flamelet library are the ratio of specific heats γ, the gas constant R and the enthalpy of formation of the mixture $\psi = \sum_{k=1}^{N} Y_k \Delta h_{f,k}^0$. The temperature is determined through Eq.(14) using the above three variables and other flow properties obtained from the flow equations. Heat release is also obtained from the flamelet library.

C. Boundary Conditions and Computational Domain

According to the experimental observations described in Refs. 37 and 38, the combustor exhibits strong flow oscillations when the inlet air temperature exceeds a threshold value and the equivalent ratio falls into the range between 0.5 and 0.7. The dominant acoustic motion in the axial direction corresponds to the first longitudinal mode, with the existence of an acoustic pressure node at the middle of the chamber. Accordingly, the computational domain shown in Fig. 3 only includes the upstream half of the chamber and the portion of the inlet annulus downstream of the swirl vane, to save computational resources.

At the inlet boundary, the mass flow rate and temperature are specified. The pressure is obtained from a one-dimensional approximation to the axial momentum equation, i.e., $\partial p / \partial x = -\rho \partial u / \partial t - \rho u \partial u / \partial x$. The mean axial-velocity distribution follows the one-seventh power law by assuming a fully developed turbulent pipe flow. The radial and azimuthal velocities are determined from the swirler vane angle. Turbulence properties at the inlet are specified by superimposing broad-band disturbances onto the mean velocity profiles. The disturbances are generated by a Gaussian-random number generator with an intensity of 15 % of the mean quantity. Since the acoustic oscillations generated in the chamber propagate upstream through the swirler, care must be exercised in specifying the acoustic boundary conditions at the inlet of the computational domain. The inlet venturi is choked and basically serves as an acoustic damper that can effectively dissipate disturbances arising from downstream.[37] Consequently, the acoustic field in the inlet section is predominated by an upstream-running wave. In the present study, an acoustic admittance function defined as

$$\hat{A}_d(\omega_n) = \frac{\hat{u}_{a,n}(\omega_n) / \overline{c}}{\hat{p}_{a,n}(\omega_n) / \overline{\gamma p}} \qquad (31)$$

is employed to characterize the response of the swirler to downstream disturbances. The instantaneous pressure and axial velocity contains contributions from the mean, turbulent, and

Fig. 3 Computational domain (total grid points: 176x141x81 =2.01x10⁶).

acoustic flowfields, i.e., $p = \overline{p} + p_t' + p_a'$ and $u = \overline{u} + u_t' + u_a'$. The acoustic pressure can be written as:

$$p_a'(t) = \sum_{1}^{L} \Re e\{\hat{p}_{a,n}(\omega_n) e^{i\omega_n t}\}$$

and the corresponding acoustic velocity can be written as:

$$u_a'(t) = (\overline{c} / \overline{\gamma p}) \sum_{1}^{L} \Re e\{\hat{A}_d(\omega_n) \hat{p}_{a,n}(\omega_n) e^{i\omega_n t}\},$$

where the admittance function $\hat{A}_d(\omega_n)$ can be obtained from an impedance-tube experiment for the swirler.[37] Generally, only a few dominating acoustic waves (which usually are the lowest order longitudinal modes) can travel upstream and need to be taken into account. In the present case, only the acoustic wave corresponding to the first longitudinal mode of the main chamber is considered because of its prevalence in the inlet.

At the outlet boundary, the characteristic conditions proposed by Poinsot and Lele[52] are applied, along with the specification of a time-invariant back pressure due to the existence of an acoustic pressure node at the middle of the chamber. This back pressure is obtained using a simplified one-dimensional momentum equation $\partial p / \partial r = \rho U_\theta^2 / r$ in the radial direction, where U_θ is the mean azimuthal velocity. The pressure at $r = 0$ is fixed as a pre-specified value. Finally, the no-slip and adiabatic conditions are enforced along all of the solid walls.

IV. Numerical Method

The resultant governing equations and boundary conditions are solved numerically by means of a density-based, finite-volume methodology. The spatial discretization employs a second-order, central-differencing scheme in generalized coordinates. A fourth-order matrix dissipation with a total-variation-diminishing switch developed by Swanson and Turkel[53] and tested by Oefelein and Yang[54] is employed to ensure computational stability and to prevent numerical oscillations in regions with steep gradients. Temporal discretization is obtained using a four-step Runge-Kutta integration scheme. A multi-block domain decomposition technique, along with static load balance, is used to facilitate the implementation of parallel computation with message passing interfaces at the domain boundaries. The theoretical and numerical framework described above has been validated against a wide variety of flow problems in order to establish its validity and accuracy.[54-57]

V. Results and Discussion

The theoretical and numerical framework described in the preceding sections was applied to an investigation of the flame dynamics in a lean-premixed swirl-stabilized combustor, as shown in Fig. 1. The baseline condition includes an equivalence ratio of 0.573 and chamber pressure of 0.463 *MPa*. The mass flow rates of methane and air are 1.71 and 50.70 *g/s*, respectively. The inlet flow velocity is 86.6 *m/s* and the corresponding Reynolds number based on the inlet flow velocity and height of the inlet annulus is 35,000. The inlet temperature of 660 *K* corresponds to the case of unstable combustion reported in Refs. 37 and 38.

The computational domain shown in Fig. 3 includes the inlet duct downstream of the swirl vanes and the upstream half of the chamber. The entire grid system has 176x141x81 points along the axial, radial, and azimuthal directions, respectively, of which 36 axial points are used to cover the inlet section. The axial and radial grids are clustered in the shear-layer regions downstream of the dump plane and near the solid walls to resolve the shear-layer and near-wall gradients. The azimuthal grids are uniformly distributed. This grid resolution was chosen based on the inlet Reynolds number such that the largest grid size falls in the inertial sub-range of the turbulent energy spectrum. The analysis was conducted on an in-house distributed-memory parallel computer. The computational domain was divided into 68 blocks, and each block was calculated on a single processor, i.e., a total number of 68 processors were used.
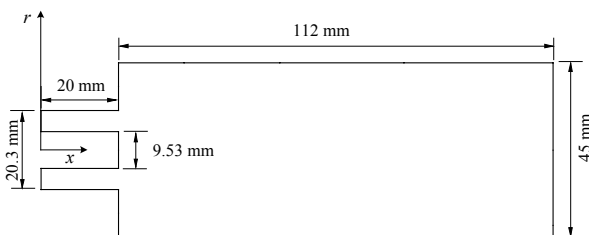
The premixed methane/air flamelet library was established using the GRI-MECH 3.0 mechanism,[58] consisting of 325 elementary reactions and 53 species. Figure 4 shows the distributions of the temperature and species-concentration fields as calculated using the CHEMKIN code.[59] The unstretched laminar flame speed is $S_L = 0.45$ m/s, and the corresponding flame thickness is 0.3 mm.

The calculated flowfield shows that the magnitude of v'/S_L ranges from 6.6 to 100 and that of l/l_F from 2.0 to 70, where the turbulent integral length scale l is approximated from the temporal correlation function based on Taylor's frozen-turbulence hypothesis. The flame is located primarily in the thin reaction zone in the premixed turbulent combustion regime diagram given in Fig. 2. The flamelet assumption employed in the present analysis is confirmed.

The Calculation was initiated by imposing broad-band velocity fluctuations at the inlet, and continued for an extended period of time until statistically meaningful data were obtained. Figure 5 shows the frequency spectra of the turbulent kinetic energy at three different locations along the inlet axis. The −5/3 law of the energy spectrum based on the Kolmogorov-Obukhow theory, which characterizes the inertia sub-range, is largely satisfied. In LES, the cutoff wave number for turbulent motions should lie in the inertia sub-range of the kinetic energy spectrum. Theses results further confirm the adequacy of the numerical grid resolution achieved.
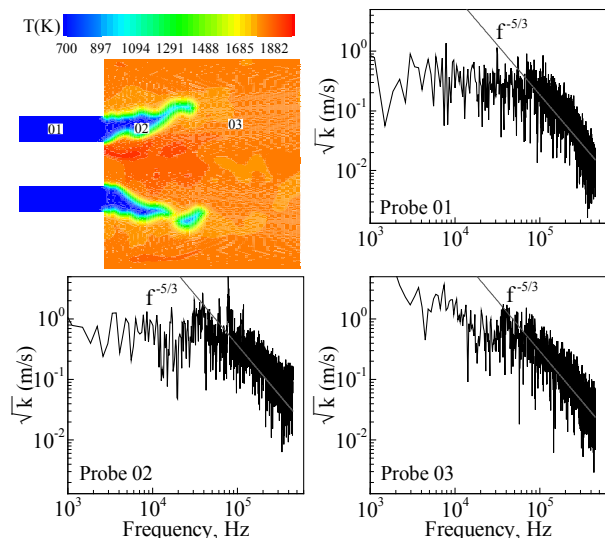
A. Flow Structures

1. Mean Flowfield

The mean flow properties are first obtained by taking a long-time average of the instantaneous quantities. In spite of significant flow motion in the azimuthal direction, the mean flowfield remains
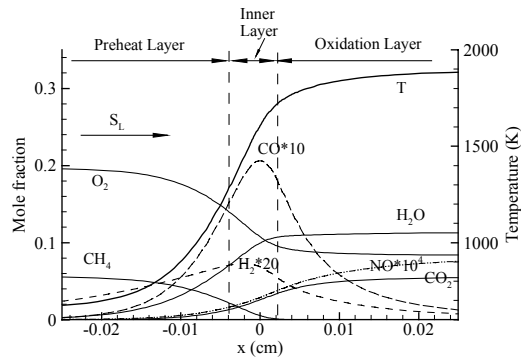
Fig 4. Temperature and species-concentration distributions of laminar premixed flame of methane and air ,ϕ = 0.573 and p = 0.463 MPa.

Fig. 5 Frequency spectra of turbulent kinetic energy at three different locations along inlet axis.

perfectly axisymmetric.[60] Figure 6 shows the mean temperature field and the pseudo-streamline pattern on the $x - r$ plane based on the mean axial and radial velocity components. A central toroidal recirculation zone (CTRZ), a form of vortex breakdown, is established in the wake of the center body under the effect of the swirling flow. It serves as a flame stabilization region where hot products are mixed with the incoming mixture of air and fuel. In addition, as a result of the sudden enlargement of the combustor configuration, a corner recirculation zone (CRZ) with two separation bubbles is formed downstream of the backward-facing step. The sizes of the CRZ and CTRZ are strongly dependent on swirl intensity, equivalence ratio, and combustor geometry.[61]

Figure 7 shows the radial distributions of the mean velocity components, pressure, and turbulent kinetic energy (TKE) at various
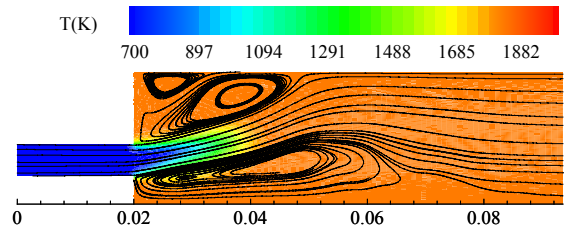
Fig.6 Mean temperature field and streamline pattern.
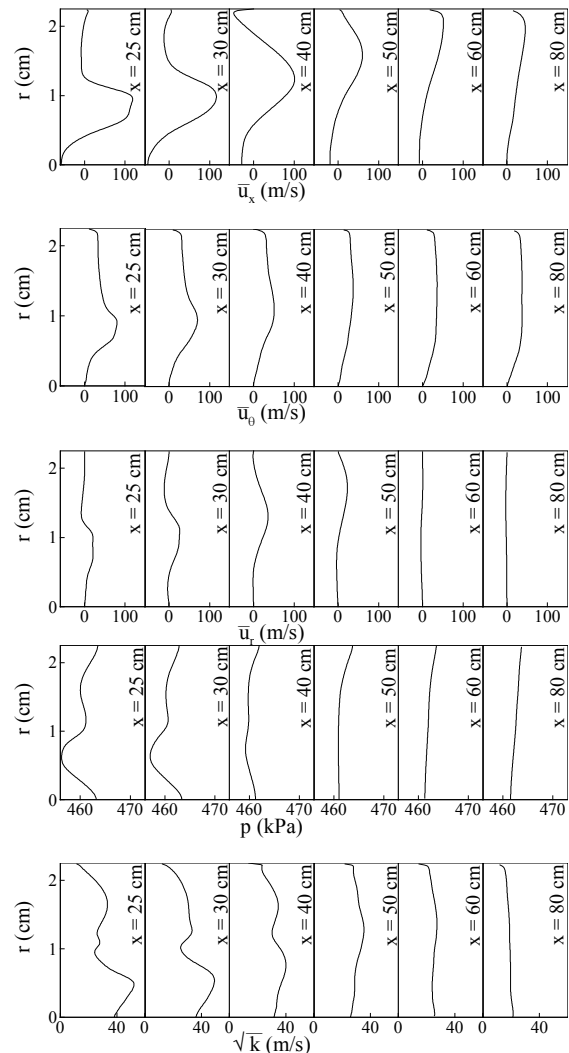
Fig.7 Radial distributions of mean velocity components, pressure and turbulent kinetic energy at various axial locations.

axial locations, where $r = 0$ corresponds to the centerline of the chamber. High swirling flow is delivered to the chamber through the inlet annulus, and decays rapidly due to the flow expansion, diffusion, and viscous dissipation. The incoming flow from the inlet annulus spreads away from the centerline under the effects of centrifugal force. Strong radial pressure gradients then arise and a low-pressure region is formed in the vicinity of the center body. As the result, a negative axial velocity region appears and a recirculation flow is established in the CRTZ. The radial distribution of the turbulent kinetic energy indicates that a high turbulence intensity region develops in the wake of the center body, where large velocity fluctuations are produced due to strong turbulent mixing between the incoming flow and the recirculating flow in the CTRZ.

2. Instantaneous Flowfield

Vorticity is of concern in the present study because of its dominant influence in determining the flow entrainment in the reaction zone and the subsequent flame evolution. Figure 8 shows a snapshot of the vorticity field on the $x - r$ and $r - \theta$ planes. Large vortical structures arise in the shear layer downstream of the dump plane and around the wrinkled flame zone. In addition to the swirler-induced vorticity, the volume dilation and baroclinic effects in the flame zone significantly contribute to the production of vorticity. Vorticies are convected downstream with accompanying irregular breaking strength (i.e., vortex breakdown), and spiral into the core region. This precessing vortex core (PVC) may resonate with the acoustic instability and induce strong flow oscillations in the chamber.

The phenomenon of vortex breakdown, defined as an abrupt change in the character of a vortex core, is manifested with the recirculation zone in the downstream of the center body. The region provides the mechanisms for flame stabilization, and is characterized by the existence of internal stagnation points and reversed flows. Lucca-Negro and O'Doherty[62] listed seven different types of vortex breakdown. Among them, bubble and spiral modes of breakdown are commonly observed in swirl-stabilized gas-turbine combustors. The bubble mode usually prevails at high swirl numbers, while the spiral mode is dominant at low swirl numbers.

Figure 9a shows the iso-surface of the vorticity field at $\omega = 75000$ $1/s$. The flow-field in the region of $r > 2$ cm is blanked to provide a clear picture of the flow structures. A vortex spiral evolves from the shear layer originating at the backward facing step due to the Kelvin-Helmholtz instabilities in both the axial and azimuthal directions.[63] This single tilted spiral structure gyrates around the centerline and persists for about two turns before breaking up into small-scale structures. The winding of the spiral is in the direction opposite to the
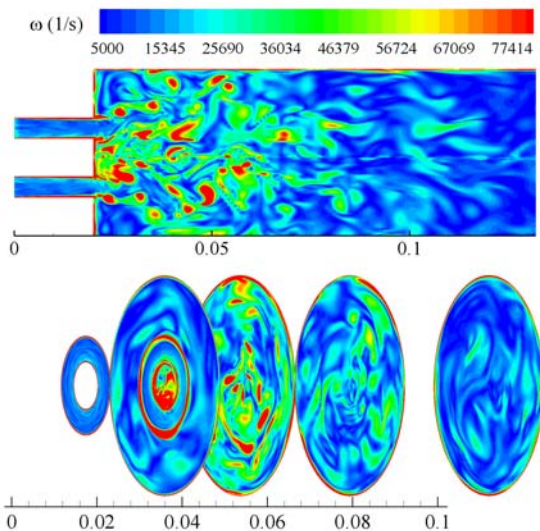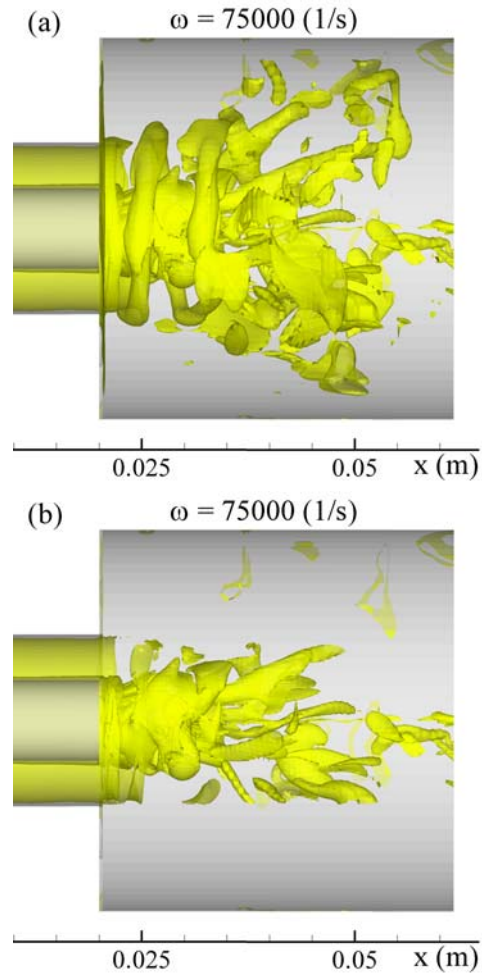
Fig. 9 Snapshot of iso-vorticity surface at ω = 75,000 s^{-1} at t = 12.34 ms (top: $r > 0.02$ m is blanked; bottom: $r > 0.01$ m is blanked).

swirling flow, which is consistent with the argument of Martin and Meiburg[64] that the counter-rotating helical waves are much more unstable in swirling flows. There still, however, remain some controversial opinions about the orientation of the spiral. The winding of the spiral has been observed to occur either in the sense of the rotation of the swirling flow, or opposite to it. No definite theory has been provided so far to explain this discrepancy.[62]

Figure 9b shows the iso-surface of the vorticity field at ω =75000 $1/s$ with the region of $r > 1$ cm blanked. An asymmetric bubble-like structure is observed with its stagnation point approaching the centerbody. It is difficult to identify a single structure due to the complex flow pattern. Both spiral and double helix structures are evidenced in connection with the presence of a precessing vortex core. According to Brucker,[65] the bubble and spiral modes of breakdown appears to be very similar, and the former can be regarded as a 'compressed' spiral.

Swirling flows are often non-axisymmetric and unstable. A PVC develops when a central vortex core starts to process around the axis of symmetry due to the helical instability. Although the PVC may improve combustion efficiency through its enhancement of turbulence intensity and mixing, it represents a largely undesired characteristic because of the possible resonant coupling with low-frequency acoustic oscillation in the combustion chamber. In the present study, two kinds of PVC, of the spiral and double-helix modes, are observed. Figure 10 shows the instantaneous streamlines on the transverse planes at three different axial locations. At $t = 11.91$ ms, a double helix mode of PVC is found with two vortex cores spiraling around the centerline, while at $t = 12.34$ ms, a single vortex core spirals around the centerline. Both the spiral and double

Fig. 8 Snapshot of vorticity magnitude field on $x - r$ and $r - \theta$ planes at t =12.34 ms.

Table 2   Acoustic Frequencies Predicted by Linear Analysis

Mode	Chamber, Hz	Inlet, Hz
1L	1,830	6,375
1T	10,678	11,065
1R	22,226	48,726
2T	17,700	21,827

t = 11.91 ms

x = 24 mm   x = 32 mm   x = 44 mm
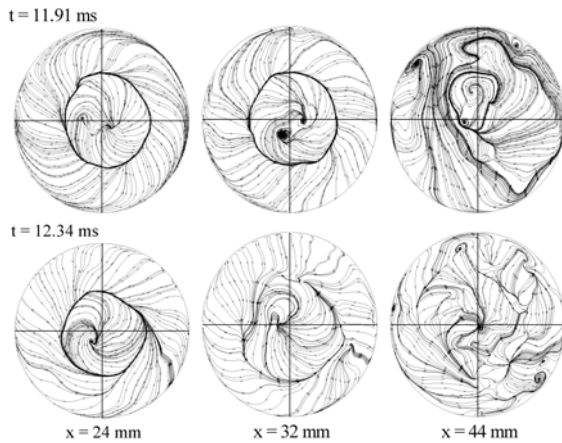
Fig. 10   Instantaneous streamlines on $r - \theta$ plane at three different locations at t = 11.91 ms and t =12.34 ms.

helix wind in a direction opposite to the main swirling flow. The mechanisms for triggering the transition between these two states are still unclear. The presence of a PVC helps explain the occurrence of instantaneous negative azimuthal velocity in the region near the centerline of the chamber.

B.   Combustion Dynamics
1. Acoustic-Mode Identification

Since the most problematic type of instability involves the coupling between acoustic motions and transient combustion response, a prerequisite of any instability research is the identification of acoustic modes in the chamber. Numerous probes were employed in the present study to register the flow oscillations in the chamber. Figure 11 shows the frequency contents of the pressure fluctuations at two different locations immediately downstream of the dump plane. Four dominant modes at the frequencies of 1795, 6852, 10,970 and 21,742 Hz are clearly observed. To facilitate data analysis and to help provide physical insight, a linear analysis of the acoustic field was performed. The inlet was assumed to be filled with a premixed combustible mixture with a speed of sound of $c = 510$ m/s, and the chamber was assumed to be filled with the burnt gases with the speed of sound of $c = 820$ m/s. An acoustically closed boundary was employed for the choked exit nozzle. The acoustic impedance of the swirler was tuned to match with the measured acoustic pressure distribution in the inlet annulus.[37] The results from the linear acoustic analysis are summarized in Table 2.

The calculated frequency of 1795 Hz corresponds to the first longitudinal (1L) mode of acoustic oscillation in the chamber, which matches closely with the measured value of 1750 Hz.[37] The slight deviation from the prediction of the linear acoustic analysis results from the uncertainties in specifying the average speed of sound and the chamber length. It is worth noting that the experimental measurements[37] also indicate the existence of the second longitudinal (2L) mode at 3500 Hz. This mode, however, was suppressed in the present numerical study, since the back pressure at the end of the computational domain was fixed at a pre-specified value, a condition that prohibited the excitation of higher modes of longitudinal oscillations. The calculated mode at 6582 Hz corresponds to the 1L mode of acoustic oscillation in the inlet annulus, and the modes at 10,970 Hz and 21,742 Hz to the first tangential (1T) and the first radial (1R) modes of the main
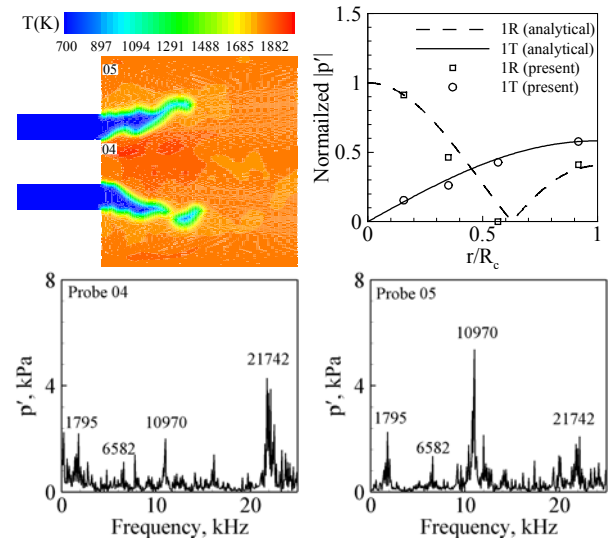
Fig.11 Power spectral densities of pressure fluctuations at two different locations and spatial distributions of 1T and 1R modes of acoustic oscillation.

chamber, respectively. Figure 11 also shows good agreement in acoustic mode shape between the calculated and the analytical results. The present analysis is capable of solving the acoustic wave motions in various parts of the domain.

2. Vortex Shedding and Acoustics Interaction

As the flow expands from the inlet annulus to the chamber, strong shear layers are formed downstream of the central body and backward-facing step. The inherent hydrodynamic instability and vortex shedding play a decisive role in determining the combustion dynamics in the chamber. When the characteristic frequencies of these processes match with those of the chamber acoustic waves, intensive interactions occur and give rise to large excursions of unsteady motions through the coupling with unsteady heat release in the flame zone.

A comprehensive review of large-scale structures in shear layers has been given by Schadow and Gutmark.[5] Instability waves develop and grow in a shear layer in its initial region. When the amplified waves reach a certain energy level, they roll up into vortices. The initial vortex-shedding frequency, f_i, also known as the most amplified frequency, can be scaled with the initial momentum thickness θ_0, and a characteristic velocity $\overline{U}$ of the shear layer. The result leads to a non-dimensional frequency or Strouhal number, $Sr_i = f_i \theta_0 / \overline{U}$. Linear instability theory for laminar mixing layers predicts this number to be close to 0.032, with $\overline{U}$ defined as the average bulk velocity $(U_1 + U_2)/2$. For a turbulent shear layer, the number changes to $Sr_i \approx$ 0.044–0.048.[66] As vortices move downstream, they merge together to oscillate at the sub-harmonics of the initial vortex shedding frequency f_i / N, with $N = 2, 3, 4 \ldots$ In most practical flows, this pairing process is terminated at some point by the finite extent of the bounding stream. Therefore there exists a cut-off frequency in the sequence of the sub-harmonics. For an axisymmetric jet, the frequency of the final sub-harmonic can be scaled with the initial diameter D and velocity U_0 of the jet.[63] The resultant preferred-mode Strouhal number is defined as: $Sr_j = f_j D / U_0$. The range of Sr_j was found to be between 0.25 and 0.5. This preferred-mode frequency f_j usually falls in the second or third sub-harmonic range of the initial frequency f_i.

Although most of the existing hydrodynamic analyses were formulated for planar flows, they can be applied with good accuracy to mixing layers in axisymmetric configurations by assuming the shear-layer thickness is very thin compared to its radius of curvature. The density differences, which may arise from combustion, are

found to have very limited effects on the most amplified frequency.[67] In the present case, the momentum thickness

$$\theta_0 = \int_0^\infty (u/U_{max})(1-u/U_{max})dy \text{ estimated from the calculated mean}$$

velocity field is 0.10 *mm*. $\overline{U} \approx 43.3$ *m/s*, $U_0 \approx 86.6$ *m/s*, and $D = (D_n - D_h)/2 = 5.385$ *mm*. If we choose $Sr_i = f_i\theta_0/\overline{U} = 0.048$, then the most amplified frequency f_i is 20,784 *Hz*. The corresponding second and third harmonic frequencies are 10,392 *Hz* and 6928 *Hz*, respectively. The Strouhal number calculated from the third sub-harmonic frequency 6928 *Hz* using $Sr_j = f_jD/U_0$ is 0.43, which is in the range of the preferred-mode Strouhal numbers. This finding suggests that the third sub-harmonic frequency is also a preferred-mode frequency. Thus, the most amplified frequency of the shear-layer instability ($f_i = 20,784$ *Hz*) matches closely with the 1R mode (21,742 *Hz*) of acoustic oscillation in the chamber, and the second sub-harmonic frequency $f_i/2 = 10,392$ *Hz* agrees with the 1T mode (10,970 *Hz*) of the chamber acoustic waves. Furthermore, the third sub-harmonic frequency (6928 *Hz*) is very close to the 1L mode (6582 *Hz*) of the acoustic waves in the inlet annulus. The strong resonance between the vortex shedding in the shear layer and acoustic motions leads to excitation of the 1R and 1T modes of the chamber and the 1L mode of acoustic waves in the inlet annulus.

3. Unstable Flame Evolution

The mean temperature field shown in Fig. 6 clearly exhibits a double-surface envelope flame anchored at the edges of the center body and the backward-facing step. This is in sharp contrast with the flame structure under stable operating conditions that shows only a single conical flame stabilized by the centerbody.[37,68,69] One major factor contributing to this phenomenon is the relatively higher inlet flow temperature in the present study as compared to that required for stable combustion. As the inlet temperature increases, the chemical induction time is shortened, and eventually reaches a level comparable to the flow residence time in the corner circulating zone downstream of the dump plane.[68,69] A flame is thus established in that region, and merges with the one originating from the centerbody. The overall flame length is substantially reduced. This situation renders the combustor more prone to instabilities according to the Rayleigh criterion, since considerable heat release occurs within a short distance close to the chamber head-end (i.e., acoustic anti-node point).

The flame dynamics can be elucidated by considering its interaction with the local oscillatory flowfield. Figure 12 presents the temporal evolution of the temperature field in the upstream of the chamber on the $x-r$ and $r-\theta$ planes over one cycle of the 1L mode of acoustic oscillation. The phase angle θ is referenced with respect to the acoustic pressure of the 1L mode at the chamber head-end. The entire process is dictated by the cold-flow entrainment into and mixing with hot gases in the vortical structures in the flame zone.

During the pressure build-up stage (around $\theta = 0^o$), the increasing pressure and favorable pressure gradient near the dump plane facilitates the delivery of the fresh reactants into the chamber. Intensive heat release then occurs after a short fluid mixing and chemical induction time. The resultant flow expansion tends to push the flame outward and simultaneously block the inlet flow at the dump plane. Unburned mixture fragments may break-up away from the main stream, and generate local hot spots when they are convected downstream. In the next stage (around $\theta = 180^o$), the decreasing pressure and adverse pressure gradient near the dump plane prevents the fresh reactants from traveling downstream in the chamber. The flame zone is thus reduced and becomes a little more compact. The temperature evolution in the transverse plane exhibits the three-dimensional structure of the flame and can be well correlated with the vorticity field shown in Fig. 8.
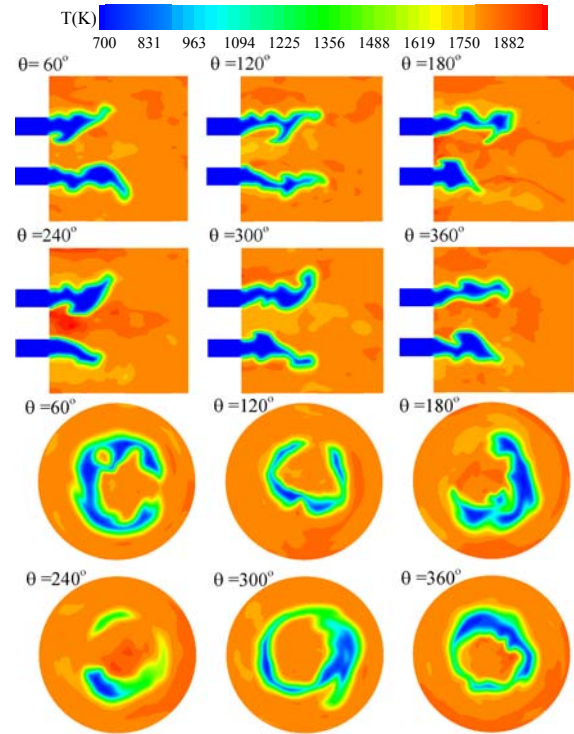
Fig. 12   Temporal evolution of temperature field on $x-r$ and $r-\theta$ planes ($x = 39.2$ mm) over one cycle of 1L mode of oscillation.

Note that the preceding description of flame motion is not precisely reflected in the temperature field shown in Fig. 12 due to the various time delays involved in the process. The qualitative trend, however, remains valid and is consistent with the distribution of the Rayleigh parameter, as will be discussed later. The detailed flame dynamics can also be studied by plotting the flame surface motion. Figure 13 presents the evolution of the isothermal surface at T=1700 *K* over one cycle of the 1L mode of acoustic oscillation, viewed from three different angles. The flame front is clearly contorted and convoluted by the spiral vortex structures, further revealing the interactions between the vortical field and the flame dynamics.

4. Vortex and Flame Interaction

The interactions between the acoustic and the shear wave motions depend on the matching of frequencies between these two types of instabilities. In the present case, the most amplified frequency of the shear wave f_i (20,784 *Hz*) is close to the 1R mode of acoustic oscillations in the chamber (21,742 *Hz*), and the first sub-harmonic frequency $f_i/2$ (10,392 *Hz*) to the 1T mode of the chamber (10,970 *Hz*). Both the 1R and 1T acoustic modes are expected to interact intimately with vortex shedding. Figure 14 shows the instantaneous vorticity field at various times within one cycle of the 1T acoustic oscillation. The thick black line indicates the flame front. Well-organized vortices are shed from the edge of the backward-facing step. The process, however, becomes much more complex downstream of the center body, due to the existence of a toroidal recirculating flow. New vortices are produced at the tip of the backward-facing step at $\theta = 72^0$, and bulge the flame front. They continue to distort the flame or even produce separated flame pockets when traveling downstream. Finally, these vortices move out of the flame region and dissipate into small-scale structures. Another set of vortices appears at $\theta = 360^0$ at the dump plane, and the cycle repeats.

To further examine the above process, the temporal evolution of the vorticity, temperature, and heat-release distributions within one cycle of the 1T mode of acoustic oscillation is plotted, as shown in Fig. 15. The vortex shedding process is clearly visualized in the evolution of the vortex spiral, which gyrates around the chamber centerline and propagates downstream. The wave-like structure on
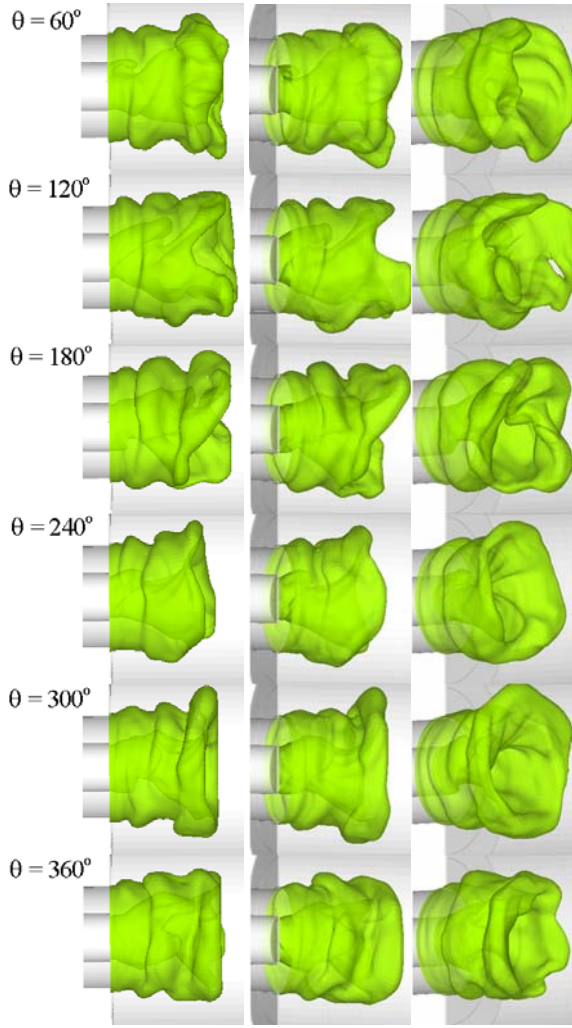
Fig. 13   Temporal evolution of iso-thermal surface at $T = 1700~K$ over one cycle of 1L mode of oscillation.
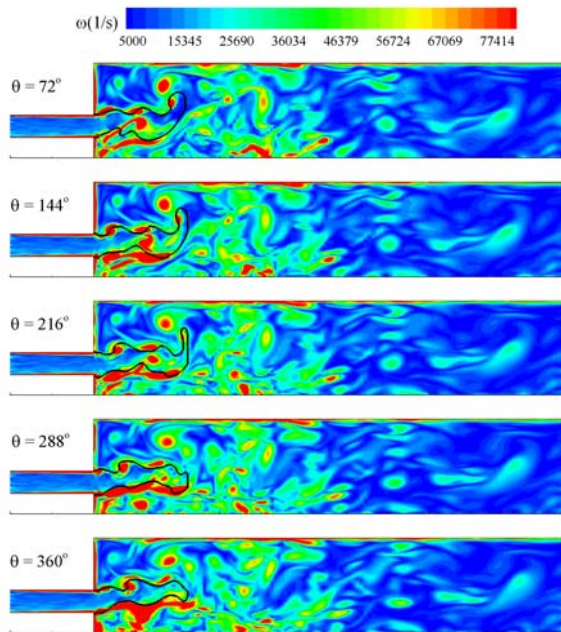

Fig 14   Vortex and flame front interaction over one cycle of 1T mode of oscillation

the flame surface possesses a characteristic frequency corresponding to the 1T acoustic wave. Because the vortex shedding affects the shapes of the flame front, it also changes the heat-release
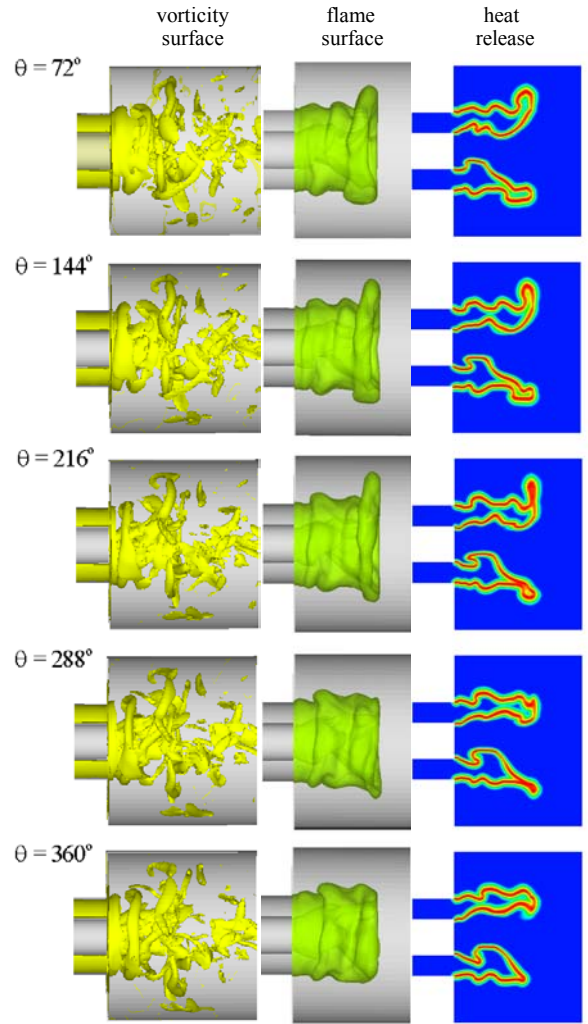

Fig.15   Temporal evolution of iso-vorticity surface at $\omega = 75{,}000~s^{-1}$ ($r > 0.02~m$ is blanked), iso-thermal surface at $T = 1700~K$ and normalized heat release contour over one cycle of 1T mode of oscillation.

distribution. As a result, the acoustic motion in the chamber is closely coupled with the heat-release fluctuation.

5.   Coupling between Acoustic and Heat-Release Oscillations

The mutual coupling between heat release and acoustic motions can be characterized using the Rayleigh parameter,[70] $Ra(\mathbf{x})$, defined as the time-averaged product of the pressure oscillation $p'(\mathbf{x},t)$ and heat-release fluctuation $q'(\mathbf{x},t)$,

$$Ra(\mathbf{x}) = \frac{1}{\tau} \int_{\tau} p'(\mathbf{x},t)q'(\mathbf{x},t)\,dt \qquad (32)$$

where τ is the time period of oscillation. The Rayleigh parameter provides a qualitative measure of the extent to which unsteady heat release drives or suppresses instabilities. The acoustic oscillation is amplified if $Ra(\mathbf{x}) > 0$, or damped out if $Ra(\mathbf{x}) < 0$. Figure 16 presents the spatial distributions of the normalized Rayleigh parameter and the mean flame position (denoted by the black line) on the $x-r$ and $r-\theta$ planes, respectively. A well-organized distribution of the Rayleigh parameter is observed, with four asymmetrical dipoles (i.e., combinations of monopoles and dipoles) located near the edge of the backward-facing step and one near the edge of the center body. These dipoles, with larger positive values on the burnt side of the flame and smaller negative values on the unburnt side, arise from the wave-like distribution of heat release shown in Fig. 15. They are closely related to the local vortical motions. The formation of these dipoles can be explained by considering the interaction between the flame and the local acoustic
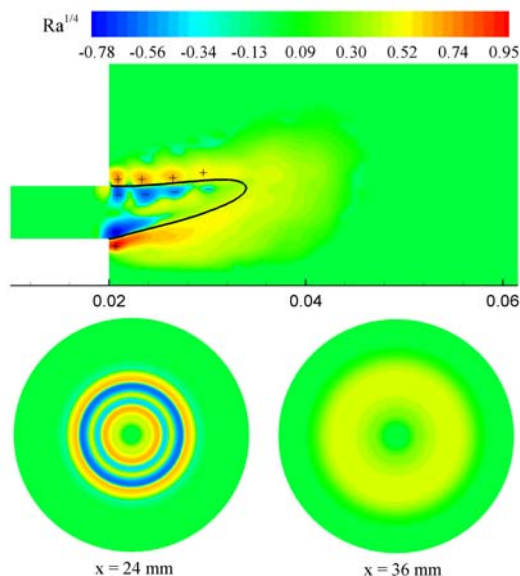
Fig 16 Distributions of normalized Rayleigh parameter on $x - r$ and $r - \theta$ planes

field. During the pressure build-up stage with a positive pressure fluctuation, the flame zone is expanded. The flame front moves into the burnt region and results in a positive heat-release fluctuation on the burnt side and a negative heat-release fluctuation on the unburnt side. In the subsequent stage with a negative pressure fluctuation, the flame zone is reduced. The flame front propagates upstream into the unburnt region and produces a negative heat-release fluctuation on the burnt side and a positive heat-release on the unburnt side. In both stages, the heat-release fluctuation is in phase with the pressure oscillation in the burnt region and results in a positive $Ra(\mathbf{x})$; however, the situation is reversed in the unburnt region and consequently results in a negative $Ra(\mathbf{x})$.

In general, the Rayleigh parameter has a positive value in much of the volume in the flame zone. The acoustic field is favorably correlated with the unsteady heat release and extracts energy from combustion. The chamber exhibits a wide range of oscillation frequencies corresponding to the natural acoustic modes in various parts of the system. The matching of certain acoustic modes and shear-layer instabilities dominates the process of vortex shedding, and consequently leads to periodic oscillations of the flame front and the ensued heat-release fluctuations. The distribution of the Rayleigh parameter reflects the coupling between heat release and acoustic waves. When such a feedback-loop process is established, energy from combustion is fed to the acoustic field and strong instabilities take place in the chamber.

VI. Conclusions

A comprehensive numerical analysis based on an LES technique has been established to investigate the combustion dynamics of a swirl-stabilized chamber. The flame dynamics and its interaction with turbulence is treated using a level-set flamelet library approach. The model provides a predictive capability for treating premixed turbulent combustion with strong swirling motions, with the acoustic flow properties solved as part of the results. As a specific example, a lean-premixed system operating in an unstable mode was carefully studied. Good agreement with analytical solutions and experimental observations was obtained in terms of the chamber acoustic characteristics and the flame shape.

Under unstable operating conditions, the flame is anchored by both the corner- and center-recirculating flows downstream of the center body and the backward-facing step, respectively. The flow-field exhibits a very complex structure, including the bubble and spiral modes of vortex breakdown and a PVC, due to the intrinsic shear-layer instability and its coupling with swirling motions. The vortical motions in the flame zone resonate intimately with the acoustic

oscillations in the chamber, and give rise to large excursions of unsteady motions. The flame is contorted and convoluted by the local flow oscillations, with the wave number of its surface structure determined by the interactions between the shear- and acoustic-wave instabilities. As a result, the energy release in the flame zone fluctuates and drives acoustic waves in the chamber. Results obtained from the present work can be used effectively to develop passive and active control strategies of combustion instabilities in gas-turbine engines.

References

[1]Correa, S.M., "A Review of NOₓ Formation under Gas-turbine Combustion Conditions," *Combustion Science and Technology,* Vol. 87, 1993, pp. 329-362.

[2]Lefebvre, A. H., "The Role of Fuel Preparation in Low-emission Combustion," *ASME Journal of Engineering for Gas Turbines and Power,* Vol. 117, 1995, pp. 617-654.

[3]Culick, F.E.C., and Yang, V., "Prediction of the Stability of Unsteady Motions in Solid Propellant Rocket Motors," Chapter 18, *Nonsteady Burning and Combustion Stability of Solid Propellants*, eds., L. DeLuca and M. Summerfield, Progress in Astronautics and Aeronautics, Vol. 143, 1992, pp. 719-779.

[4]Culick, F.E.C., and Yang, V., "Overview of Combustion Instabilities in Liquid-Propellant Rocket Engines," Chapter 1, *Liquid Rocket Engine Combustion Instability*, eds., V. Yang and W. E. Anderson, Progress in Astronautics and Aeronautics, Vol. 169, 1995, pp. 3-37.

[5]Schadow, K.C. and Gutmark, E., "Combustion Instability Related to Vortex Shedding in Dump Combustor and Their Passive Control," *Progress in Energy and Combustion Science*, Vol. 18, 1992, pp. 117-132.

[6]Lieuwen, T. and Zinn, B.T. "The Role of Equivalence Ratio Oscillation in Driving Combustion Instabilities in Low Nox Gas Turbines," *Proceedings of the Combustion Institute*, Vol. 27, 1998, pp. 1809-1816.

[7]Shtern, V. and Hussain, F., "Collapse, Symmetry Breaking, and Hysteresis in Swirling Flows," *Annual Review of Fluid Mechanics,* Vol. 31, 1999, pp. 537-566.

[8]Paschereit O.C., Gutmark E. and Weisenstein W., "Excitation of Thermoacoustic Instabilities by Interaction of Acoustics and Unstable Swirling Flow," *AIAA Journal,* Vol. 38, No.6, 2000, pp. 1025-1034.

[9]Menon, S. and Jou, W.H., "Large-Eddy Simulation of Combustion Instability in an Axisymmetric Ramjet Combustor," *Combustion Science and Technology*, Vol. 75, 1991, pp. 53-72.

[10]Kailasanath, K., Gardner, J.H., Oran, E.S. and Boris, J.P., "Numerical Simulation of Unsteady Reactive Flows in a Combustion Chamber," *Combustion and Flame*, Vol. 86, July 1991, pp. 115-134.

[11]Thibaut, D. and Candel, S., "Numerical Study of Unsteady Turbulent Premixed Combustion: Application to Flashback Simulation," *Combustion and Flame,* Vol. 113, April 1998, pp. 53-65.

[12]Schonfeld T. and Poinsot T., "Influence of Boundary Conditions in LES of Premixed Combustion Instabilities," *Annual Research Briefs*, Center for Turbulence Research, Stanford University, 1999.

[13]Kim, W.W., Menon, S. and Mongia, H.C., "Large Eddy Simulation of a Gas Turbine Combustor Flow," *Combustion Science and Technology,* Vol. 143, 1999, pp. 25-62.

[14]Angelberger, C., Veynante, D. and Egolfopoulos, F., "LES of Chemical and Acoustic Forcing of a Premixed Dump Combustor," *Flow, Turbulence and Combustion,* Vol. 65, 2000, pp. 205-222

[15]Fureby, C., "A Computational Study of Combustion Instabilities due to Vortex Shedding," *Proceedings of the Combustion Institute*, Vol. 28, 2000, pp. 783-791.

[16]Wang, S.W., Hsieh S.Y. and Yang, V., "An LES Study of Unsteady Flow Evolution in Swirl Injectors with external excitations," *Proceedings of 3rd International Symposium on Turbulence and Shear Flow Phenomena,* Sendai, Japan, June, 2003, pp. 905-910.

[17]Candel, S., Thevenin, D., Darabiha, N. and Veynante D., "Progress in Numerical Combustion", *Combustion Science and Technology,* Vol. 149, 1999, pp. 297-337.

[18]Charlette, F., Meneveau, C. and Veynante, D., "A Power-Law Flame Wrinkling Model for LES of Premixed Turbulent Combustion. Part I: Non-Dynamic Formulation and Initial Tests," *Combustion and Flame*, Vol. 131, Oct. 2002, pp. 159-180.

[19]Boger, M., Veynante, D., Boughanem, H. and Trouve, A., "Direct Numerical Simulation Analysis of Flame Surface Density Concept For Large Eddy Simulation of Turbulent Premixed Combustion," *Proceedings of the Combustion Institute*, Vol. 27, 1998, pp. 917-925.

[20]Peters, N., *Turbulent Combustion*. Cambridge University Press, Cambridge, U.K., 2000.

[21]Hawkes, E.R. and Cant, R.S., "Implications of a Flame Surface Density Approach to Large Eddy Simulation of Premixed Turbulent Combustion," *Combustion and Flame*. Vol. 126, Aug. 2001, pp. 1617-1629.

[22]Fureby, C. and Lofstrom, C., "Large Eddy Simulation of Bluff Body Stabilized Flames", *Proceedings of the Combustion Institute*, Vol. 25, 1994, pp. 783-791.

[23]Fureby, C. and Moller, S.I., "Large Eddy Simulation of Reacting Flows Applied to Bluff Body Stabilized Flames," *AIAA Journal,* Vol. 33, No.12, 1995, pp. 2339-2347.

[24]Moller, S.I., Lundgren, E. and Fureby, C., "Large Eddy Simulation of Unsteady Combustion," *Proceedings of the Combustion Institute*, Vol. 26, 1996, pp. 241-248.

[25]Colin, O., Ducros, F., Veynante, D. and Poinsot, T., "A thickened Flame Model for Large Eddy Simulation of Turbulent Premixed Combustion," *Physics of Fluids,* Vol. 12, 2000, pp. 1843-1863.

[26]Chakravarthy, V.K. and Menon, S., "Subgrid Modeling of Turbulent Premixed Flames in the Flamelet Regime," *Flow, Turbulence and Combustion,* Vol. 65, 2000, pp. 133-161.

[27]Chakravarthy, V.K. and Menon, S., "Large-Eddy Simulation of Turbulent Premixed Flames in the Flamelet Regime," *Combustion Science and Technology,* Vol. 162, 2001, pp. 175-222.

[28]Hawkes, E.R. and Cant, R.S., "A Flame Surface Density Approach to Large Eddy Simulation of Premixed Turbulent Combustion," *Proceedings of the Combustion Institute*, Vol. 28, 2000, pp. 51-58.

[29]Weller, H., Tabor, G., Gosman, A.D. and Fureby,C., "Application of a Flame-Wrinkling LES Combustion Model to a Turbulent Mixing Layer," *Proceedings of the Combustion Institute*, Vol. 27, 1998, pp. 899-907.

[30]Fureby, C., "Large Eddy Simulation of Combustion Instabilities in a Jet Engine Afterburner Model," *Combustion Science and Technology*, Vol. 161, 2000, pp. 213-243.

[31]Flohr, P. and Pitsch, H. "A Turbulent Flame Speed Closure Model for LES of Industrial Burner Flows," *Proceedings of the Summer Program*, Center for Turbulence Research, Stanford University, 2000.

[32]Charlette, F., Meneveau, C. and Veynante, D., "A Power-Law Flame Wrinkling Model for LES of Premixed Turbulent Combustion. Part II: Dynamic Formulation," *Combustion and Flame*, Vol. 131, Oct. 2002, pp. 181-197.

[33]Herrmann, M., "Numerical Simulation of Premixed Turbulent Combustion Based on a Level Set Flamelet Model," Ph. D. Thesis, der Rheinisch-Westfalischen Technischen Hochschule Aachen, Germany, 2000.

[34]Nilsson, P. and Bai, X.S., "Level-Set Flamelet Library Approach for Premixed Turbulent Combustion," *Experimental Thermal and Fluid Science,* Vol. 21, 2001, pp. 87-98.

[35]Duchamp, de Lageneste, L. and Pitsch, H., "A Level Set Approach to Large Eddy Simulation of Premixed Turbulent Combustion," *Annual Research Briefs*, Center for Turbulence Research, Stanford University, 2000.

[36]Pitsch, H. and Duchamp, de Lageneste, L., "Large Eddy Simulation of Premixed Turbulent Combustion Using a Level-set Approach," *Proceedings of the Combustion Institute*, Vol. 29, 2002, pp. 2001-2008.

[37]Broda, J.C., Seo, S., Santoro, R.J., Shirhattikar, G. and Yang, V., "An Experimental Study of Combustion Dynamics of a Premixed Swirl Injector," *Proceedings of the Combustion Institute*, Vol. 27, 1998, pp. 1849-1856.

[38]Lee S.-Y., Seo, S., Broda, J.C., Pal, S. and Santoro R.J., "An Experimental Estimation of Mean Reaction Rate and Flame Structure during Combustion Instability in a Lean Premixed Gas Turbine Combustor," *Proceedings of the Combustion Institute*, Vol. 28, 2000, pp. 775-782.

[39]Gupta, A.K., Lilley, D.G., Syred, N., *Swirl Flows*, Abacus Press, London, 1984.

[40]Oefelein, J.C. and Yang, V., *Recent Advances in Spray Combustion* (*II*), Progress in Astronautics and Aeronautics, Vol. 171, Washington, DC, 1996, pp. 263-304.

[41]Erlebacher, G., Hussaini, M.Y., Speziale, C.G. and Zang, T.A., "Toward the Large Eddy Simulation of Compressible Turbulent Flows," *Journal of Fluid Mechanics*, Vol. 238, 1992, pp. 155-158.

[42]Pope, S.B., *Turbulent Flows*, Cambridge University Press, Cambridge, U.K., 2000.

[43]Williams, F.A. *Combustion Theory*, Second ed., Addison-Wesley Publishing Company, California, 1985.

[44]Clavin, P., "Dynamic Behavior of Premixed Flame Fronts in Laminar and Turbulent Flows," *Progress in Energy and Combustion Science*, Vol. 11, 1985, pp. 1-59.

[45]Law, C.K. and Sung, C.J., "Structure, Aerodynamics and Geometry of Premixed Flamelets," *Progress in Energy and Combustion Science*, Vol. 26, 2000, pp. 459-505.

[46]Lipatnikov, A.N. and Chomiak, J., "Turbulent Flame Speed and Thickness: Phenomenology, Evaluation and Application in Multi-dimensional Simulations," *Progress in Energy and Combustion Science*, Vol. 28, 2000, pp. 1-74.

[47]Wirth, M., Keller, P., and Peters, N., "A Flamelet Model for Premixed Turbulent Combustion in SI-Engines," *SAE Paper* 932646, 1993.

[48]Plessing, T., Mansour, M.S., Peters, N. and Cheng, R.K., "Ein Neuartiger Niedrig-drallbrenner zur Untersuchung turbulenter Vormischflammen," *VDI-Berichte*, Vol. 1492, 1999, pp. 457-462.

[49]Sussman, M., Smereka, P. and Osher, S., "A Level Set Approach for Computing Solutions to Incompressible Two-Phase Flow," *Journal of Computational Physics,* Vol. 114, Sept. 1994, pp. 146-163.

[50]Russo, G. and Smereka, P., "A Remark on Computing Distance Functions," *Journal of Computational Physics,* Vol. 163, Sep. 2000, pp. 51-67.

[51]Sethian, J.A., *Level Set Methods and Fast Marching Methods*, Cambridge University Press, Cambridge, U.K., 1999.

[52]Poinsot, T. and Lele S., "Boundary Conditions for Direct Simulation of Compressible Viscous Flows," *Journal of Computational Physics*, Vol. 101, July 1992, pp. 104-129.

[53]Swanson, R.C. and Turkel, E., "On Central Difference and Upwind Schemes," *Journal of Computational Physics*, Vol. 101, 1992, pp. 292-306.

[54]Oefelein, J.C. and Yang, V., "Modeling High-Pressure Mixing and Combustion Processes in Liquid Rocket Engines," *Journal of Propulsion and Power,* Vol. 14, No. 5, 1998, pp. 843-857.

[55]Sung, H.G., "Unsteady Flowfield in an Integrated Rocket Ramjet Engine and Combustion Dynamics of a Gas Turbine Swirl-stabilized Injector," *Ph.D. Thesis*, Department of Mechanical Engineering, The Pennsylvania State University, University Park, PA, Dec. 1999.

[56]Apte, S. and Yang, V., "Unsteady Flow Evolution in Porous Chamber with Surface Mass Injection, Part 1: Free Oscillation," *AIAA Journal,* Vol. 39, No. 8, 2001, pp. 577-1586.

[57]Wang, S.W., "Vortical Flow Dynamics and Acoustic Response of Gas-Turbine Swirl-Stabilized Injectors," *Ph.D. Thesis*, Department of Mechanical Engineering, The Pennsylvania State University, University Park, PA, Oct. 2003.

[58]Gregory P. Smith, David M. Golden, Michael Frenklach, Nigel W. Moriarty, Boris Eiteneer, Mikhail Goldenberg, C. Thomas Bowman, Ronald K. Hanson, Soonho Song, William C. Gardiner, Jr., Vitali V. Lissianski, and Zhiwei Qin. http://www.me.berkeley.edu/gri_mech/

[59]Kee, J.R., Rupley, F.M., and Miller, J.A., "Chemkin-ii a Fortran Chemical Kinetics Package for the Analysis of Gas Phase Chemical Kinetics," Technical Report SAND89-8009B, Sandia National Laboratories, Livermore, CA, 1992.

[60]Panda, J. and McLaughlin, D.K., "Experiments on the Instabilities of a Swirling Jet," *Physics of Fluids,* Vol. 6, Jan. 1994, pp. 263-276.

[61]Wang, T., "Modeling of Combustion Dynamics in Gas Turbine Engines," *Ph.D. Thesis*, Department of Mechanical Engineering, The Pennsylvania State University, University Park, PA, Dec. 1997.

[62]Lucca-Negro, O. and O'Doherty, T., "Vortex Breakdown: a Review," *Progress in Energy and Combustion Science*, Vol. 27, 2001, pp. 431-481.

[63]Coats, C.M., "Coherent Structures in Combustion," *Progress in Energy and Combustion Science,* Vol. 22, 1996, pp. 427-509.

[64]Martin, J.E. and Meiburg, E., "Nonlinear Axisymmetric and Three Dimensional Vorticity Dynamics in a Swirling Jet Model," *Physics of Fluids*, Vol. 8, July 1996, pp. 1917-1928.

[65]Brücker, C., "Study of Vortex Breakdown by Particle Tracking Velocimetry. Part 2: Spiral-type Vortex breakdown," *Experiments in Fluids,* Vol. 14, 1993, pp. 133-139.

[66]Ho, C.M. and Huerre, P., "Perturbed Free Shear Layer," *Annual Review of Fluid Mechanics,* Vol. 16, 1984, pp. 365-424.

[67]Soteriou, M.C. and Ghoniem, A.F., "Effects of the Free-Stream Density Ratio on Free and Forced Spatially Developing Shear Layers," *Physics of Fluids*, Vol. 7, Aug. 1995, pp. 2036-2051.

[68]Huang, Y. and Yang, V., "Bifurcation of Flame Structure in a Lean-Premixed Swirl-Stabilized Combustor: Transition from Stable to Unstable Flame," *Combustion and Flame* (Accepted for publication), 2003.

[69]Huang, Y. and Yang, V., "Unsteady Flow Evolution and Flame Dynamics in a Lean-Premixed Swirl-Stabilized Combustor," *Proceedings of 3rd International Symposium on Turbulence and Shear Flow Phenomena,* Sendai, Japan, June, 2003, pp.1019-1024.

[70]Rayleigh, J.W.S., *The Theory of Sound*, Vol. 2, Dover, New York, 1945, pp.224-235.